Available online at www.sciencedirect.com
ScienceDirect
Journal of Nuclear Materials 360 (2007) 196–207
journal of nuclear materials
www.elsevier.com/locate/jnucmat

Hydrogen and helium trapping in tungsten under single and sequential irradiations

H.T. Lee, A.A. Haasz *, J.W. Davis, R.G. Macaulay-Newcombe

University of Toronto Institute for Aerospace Studies, 4925 Dufferin Street, Toronto, ON, Canada M3H 5T6

Received 17 May 2006; accepted 26 September 2006

Abstract

The trapping of hydrogen and helium in polycrystalline tungsten irradiated with 500 eV He^+, H^+ and D^+ ions, individually or sequentially, has been measured by thermal desorption spectroscopy. Specimens irradiated with 500 eV He^+ at 300 K show three He release peaks in the vicinity of ~500, ~1000, and ~1200 K. The helium is thought to form He vacancy complexes or bubbles. Increasing the specimen temperature to 700 K does not significantly affect the trapping behavior of He. Sequential He^+–D^+ irradiation at 300 K results in the elimination of He release above 800 K. Instead, both D and He were released in the range 400–800 K. This is interpreted as interstitial D and He released from the near surface. Sequential He^+–D^+ irradiation at 700 K resulted in a reduced single He peak at ~1000 K with very little release observed below 800 K; no D was trapped for irradiations at 700 K. Sequential D^+–He^+ irradiations at 300 K show that He trapping occurs in much the same manner as for the He^+-only case while D retention is reduced at the near surface. Sequential D^+–He^+ irradiations at 700 K indicate that pre-irradiation with D^+ has little or no effect on the subsequent trapping behavior of He.

PACS: 28.52.Fa; 79.20.Rf; 61.80.Jh; 61.82.Bg

1. Introduction

Tungsten is a primary candidate for the high flux, low ion-energy region of the divertor in ITER [1]. It has good thermal properties (i.e., high melting point and good thermal conductivity) as well as a low sputtering yield for minimizing impurity generation. Under burning plasma conditions, tungsten will be irradiated with the hydrogen fuel (T and D) and helium. Since He is a closed-shell inert gas, it interacts repulsively with metal atoms and is considered essentially insoluble in all metals [2]. Therefore, He irradiation often leads to blister formation and subsequent degradation of the mechanical properties of metals [3]. Such material modifications may alter the hydrogen retention and recycling properties of W, affecting the particle balance responsible for plasma fuelling and tritium inventory. Earlier studies of He trapping in W include references [4–6] with subsequent reviews of He in metals in references [7–9]. More recently, helium retention, damage evolution, and blistering in tungsten have been studied

* Corresponding author. Tel.: +1 416 6677734; fax: +1 416 6677799.
E-mail address: tonyhaasz@utias.utoronto.ca (A.A. Haasz).

0022-3115/$ - see front matter © 2006 Elsevier B.V. All rights reserved.
doi:10.1016/j.jnucmat.2006.09.013

as a function of incident He energy, fluence, as well as specimen temperature [10–15]. The database for hydrogen interactions with tungsten has also been growing steadily, e.g., [16–19]. However, only limited experimental data aimed at understanding the interaction between hydrogen and helium in tungsten exist [20–23].

The objective of this work was to study: (i) He trapping in W for He^+-only irradiations, (ii) the effect of deuterium on He trapping in W for sequential D^+–He^+ irradiations, and (iii) the effect of He on hydrogen (deuterium) trapping in W for sequential He^+–$H^+(D^+)$ irradiations.

2. Experiment

2.1. Specimen

Polycrystalline tungsten specimens (PCW) measuring $8 \times 10\ mm^2$ were cut from the same sheet of 25 μm thick foil. The manufacturer (Rembar Corp.) quoted the purity as 99.96 wt% with the main impurities being Mo (<100 ppm), C (<30 ppm), and O (<30 ppm). The grain size of this PCW material, based on scanning electron microscopy (SEM) surface analysis, was seen to be about 5–10 μm [18]. Prior to irradiation the specimens received no surface preparation in the form of mechanical or electropolishing, but were annealed at 1500 K in vacuum for 30 min. The nominal pressure during annealing was 2×10^{-7} Torr. The annealed specimens were then exposed to air for typically weeks prior to irradiation, resulting in a cloudy finish on the surface. Secondary ion mass spectroscopy (SIMS) analysis indicated that this cloudy appearance is due to the presence of a near surface layer (<3 nm thickness) containing O and WO_3; see profiles (1) and (3) in Fig. 1(a). This can be assumed to be the initial surface condition of all specimens used in this study prior to irradiation. It is expected that this thin layer will be removed during ion irradiations. Following irradiation, with 500 eV D^+-only at 300 K (fluence of $10^{23}\ D^+/m^2$), the implanted area exhibits the presence of O and WO_3 to a deeper depth of ~7 nm; beyond which the O and WO_3 concentrations drop off significantly – see profiles (1) and (3) in Fig. 1(b).

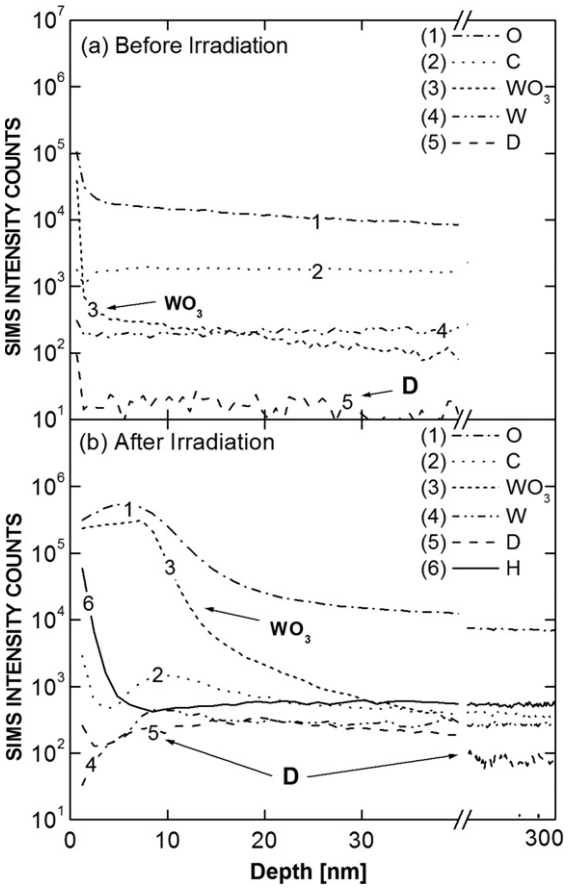

Fig. 1. SIMS depth profiles for 500 eV D^+-only irradiations at 300 K with a fluence of $10^{23}\ D^+/m^2$ (a) before irradiation and (b) after irradiation.

2.2. Hydrogen and helium irradiations

All irradiations were performed in an ultra-high vacuum dual-beam ion accelerator facility with both beams at 21° from normal incidence to the test specimen. The beams were mass analyzed and their energies and fluxes were controlled independently [24]. The background pressure was typically $\sim 10^{-8}$ Torr before irradiation and $\sim 10^{-7}$ Torr during irradiation. In order to reduce the spatial beam flux variations, only the central part of the beam(s) was allowed to impact the specimen. This was achieved by clamping a W foil mask with a 1.5 mm diameter aperture in front of the specimen. A 25 μm thick strip of mica with a 2 mm diameter aperture was placed between the mask and the specimen to allow the beam current on the specimen to be measured directly. The specimen was heated with a ceramic heater and its temperature during irradiation was measured with a chromel–alumel thermocouple.

The irradiations were performed with 2 keV He^+ and 3 keV $D_3^+(H_3^+)$ ions. The specimens were biased to +1500 V resulting in energies of 500 eV per D, H, and He atom. Typical fluxes were $10^{19}\ D^+(H^+)/m^2\ s$

and 10^{18}–10^{19} He^+/m^2 s. The ion beams were first focused onto a beam stop and adjusted to give the desired ion flux before commencing specimen irradiation. For sequential (SEQ) He^+–D^+ and D^+–He^+ irradiations, the quadrupole mass spectrometer (QMS) could not distinguish the small mass difference between released He and D_2 during thermal desorption. (^{4}He: $m = 4.0026$ amu and D_2: $m = 4.0282$ amu.) Therefore, separate SEQ He^+–H^+ irradiations were performed to extract the He trapping behavior. The SEQ He^+–H^+ profiles were then subtracted from SEQ He^+–D^+ irradiations to extract the D trapping behavior. This is illustrated in Figs. 5 and 7, and further discussed in Sections 4.1 and 4.3. Since, no SEQ H^+–He^+ irradiations were performed, He^+-only irradiations were subtracted from the SEQ D^+–He^+ cases to approximate the D trapping behavior. This is illustrated in Figs. 7 and 8, and further discussed in Sections 4.2 and 4.3. It was assumed that the H and D behave and interact the same way with helium and tungsten. The time delay between irradiations for the two ion species during SEQ irradiations was typically less than 2 s. In the 300 K irradiation cases, the specimens were then held in vacuum for 1 h before being removed. For the 700 K cases, most of the specimens were held at 700 K in vacuum for 1 h following irradiation and then cooled at ~100 K/min.; they are marked by (τ) in the figures.

2.3. Thermal desorption spectroscopy (TDS)

To minimize the background and to ensure that the mask did not interfere during desorption, TDS was performed in a separate vacuum system, with delays of typically one week between irradiation and desorption. The effect of post-irradiation air exposure – and possible oxide formation – was investigated by Quastel et al. [25]. For experimental procedures similar to the ones used in the present study, the air exposure did not substantially affect the measured D retention and desorption profile compared to a case where the post-implantation wait period occurred in vacuum. Although no similar data exist for the effect of air exposure on He retention, it is not unreasonable to expect the effect to be similar to the D case.

Following the post-irradiation delay time, tungsten–rhenium thermocouple wires were spot-welded to the specimen, typically 2–3 mm away from the beam spot. The specimen was then installed onto a tungsten heating cradle and the system was pumped until a base pressure of $\sim 2 \times 10^{-8}$ Torr was reached. The TDS chamber, with the specimen in it, was baked to ~380 K prior to desorption for all 500 eV He^+-only and SEQ irradiation cases at 300 K (excluding profiles (2) in Figs. 3 and 8); following the procedure of Poon et al. [17,26]. The effect of chamber baking on the thermal desorption profiles and total retention are further discussed below.

During TDS, all specimens were then heated linearly (temperature-wise) to 1500 K and held there for 2 min. Temperature ramping rates during thermal desorption were 2.1–3.6 K/s. The reproducibility of the TDS peak locations for the ramping rates used is within ±10 K at desorption temperatures <700 K and within ±50 K at temperatures >700 K; compare profiles (1) and (2) in Fig. 2. The exception is the ~1200 K peak which only occurs for some cases – similar shifts (±100 K) have been observed in parallel studies [27,28] and a potential cause for this peak is suggested in Section 3.2. For the entire TDS spectra, it is noted that an increase in ramping rate (from 2.1 to 3.6 K/s) resulted in increased release rates but the shift in peak locations were within experimental reproducibility; see above. The total He and D retention were independent of ramping rates as was also observed by Poon [26].

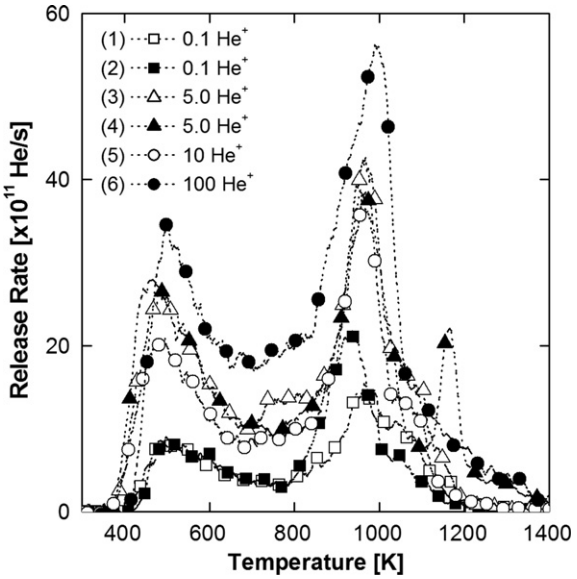

Fig. 2. TDS profiles for 500 eV He^+ irradiations at 300 K. Temperature ramping rates varied from 2.1 to 3.6 K/s. Profiles (1) and (2): 2.6 K/s; (3) and (5): 2.1 K/s; (4) and (6): 3.6 K/s. (Legend: fluences in units of $\times 10^{22}/m^2$).

The amount of He retained in the specimen for He^+-only and SEQ He^+–H^+ irradiations was determined by integrating the mass-4 QMS signal (which is all due to He) during thermal desorption. The QMS was calibrated in situ using a standard He leak bottle. D retention was derived by taking the sum of the following two components: (i) The directly measured HD molecules (mass-3 QMS signal) formed by the released D from the specimen and the H in the desorption chamber and (ii) the amount of D_2 molecules obtained by taking the difference in mass-4 QMS signals between He^+–H^+ and He^+–D^+ irradiations. Typically, HD contributed ~2–5% and D_2 ~95–98% to the total D retention. For SEQ D^+–He^+ the D contribution can only be approximated since no SEQ H^+–He^+ irradiations were performed. Instead, the He^+-only spectra were subtracted from the SEQ D^+–He^+. In this approximation, HD accounted for ~10% and D_2 for ~90% of the total D retention. For D retention calculations, all QMS signals were calibrated to a known deuterium leak. For H^+-implanted specimens, due to the excessive H_2 background in the TDS chamber, the amount of H released from the specimens during TDS could not be separated from the background. Therefore, no H desorption profiles and H retention data were obtained.

The reproducibility of the measured He retention varied with incident fluence: from ±18% (for fluences of $\sim 10^{21}$ He^+/m^2) to ±2% (for 5×10^{22} He^+/m^2). A 20% reduction in He retention due to the chamber baking process is observed for an implanted fluence of 5×10^{22} He^+/m^2; compare data (1) and (2) in Fig. 3. At this fluence, the effect of chamber baking can be clearly distinguished from experimental error. However, for the lower fluence cases, we make no specific differentiation since the differences were within the range of experimental reproducibility (±18%).

The reproducibility of the measured D retention was ±15% for an incident fluence of $\sim 10^{23}$ D^+/m^2 – similar to previous experiments using similar procedures [25,26]. TDS chamber baking resulted in a 40% reduction in D retention in the present study; as was also observed in experiments with in situ irradiation and TDS [25]. Since all of the present SEQ irradiations at 300 K were done with chamber baking, we have also obtained desorption measurements with chamber baking for 300 K D^+-only irradiations in this study for comparison purposes; see profile (10) in Fig. 5. No chamber baking was used for SEQ irradiations at 700 K.

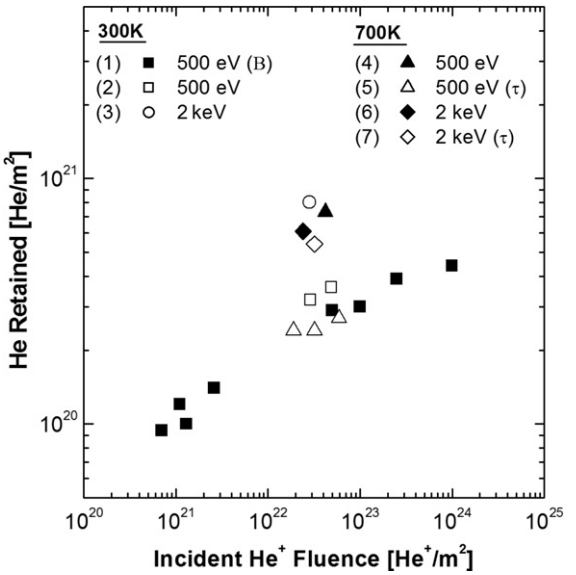

Fig. 3. He retention as a function of incident He^+ fluence for 500 eV and 2 keV He^+. Profiles labeled with (τ) correspond to specimens held at 700 K for 1 h following implantation at 700 K. Solid square data (1) correspond to TDS with the chamber baked (B) at ~380 K prior to desorption; the other irradiations in this figure were performed without chamber baking. The temperature ramping rates varied between 2.1 and 3.6 K/s.

3. Results and discussion: He^+-only irradiations

3.1. He^+-only irradiations at 300 K

Thermal desorption spectra for helium implanted in PCW at 300 K for fluences 10^{21}–10^{24} He^+/m^2 are shown in Fig. 2. The positions of the desorption peaks vary only a little for the different fluences, with two major peaks seen at ~500 and ~1000 K. For one of the 5×10^{22} He^+/m^2 fluence cases (profile (4)), a third peak at ~1200 K was also observed. None of the other specimens implanted at 300 K exhibited this third peak; however, release peaks at this temperature were also seen with He^+-only (Fig. 4) and sequential D^+–He^+ (Fig. 11) irradiations at 700 K. The ~1200 K peak was also observed in a parallel study on simultaneous irradiations of similar PCW specimens by He^+–H^+ and He^+–D^+ at both 300 and 700 K [27,28].

Release peaks at ~500 K have been observed by several authors in both single-crystal tungsten at lower He^+ fluences [5] and PCW using keV He^+ ions [13] at fluences similar to the present study. Release from surface sites [4,5] and impurity locations [6] has been proposed, yet this present some inconsistencies when applied to the present results. First,

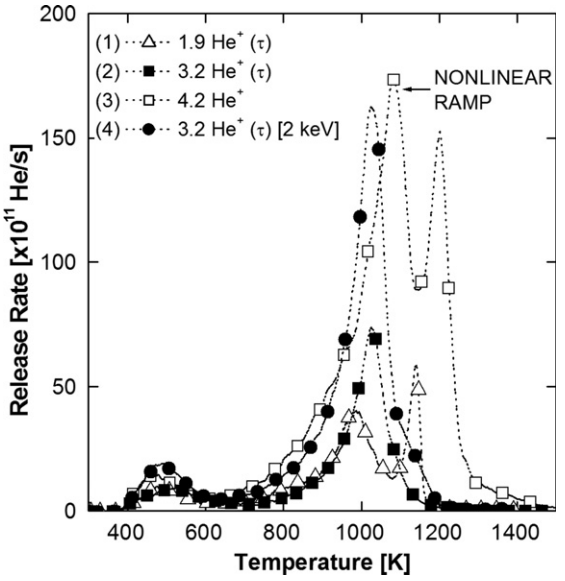

Fig. 4. TDS profiles for 500 eV He^+ irradiations at 700 K. Temperature ramping rates were in the range 2.7–3.2 K/s. The TDS profile for 2 keV He^+ irradiation is also shown for comparison. Profiles labeled with (τ) correspond to specimens held at 700 K for 1 h following irradiation at 700 K. The peaks of profile (3) were shifted to higher temperature due to increasing nonlinear ramping rate during desorption. (Legend: fluences in units of $\times 10^{22}/m^2$).

while Erents and Carter [29] have observed the disappearance of this peak following post-irradiation with Kr^+ ions, post-irradiations with hydrogen in the present study failed to remove it (see Section 4.1). While this may be due to the different target sputtering yields, it is also possible that He release at ~500 K may not be confined to surface sites alone. Second, trapping at metallic impurities have shown several release peaks within the range 500–900 K [6]. Yet in Fig. 2, no clear peaks are discernible within this range. Therefore, we postulate that the release at ~500 K may be from He clusters at grain boundaries and within the crystal, possibly at dislocation loops near helium-vacancy (He_nV_m) complexes.

The release peak at ~1000 K has also been observed in past studies and is associated with He release from a vacancy site filled with 5–10 He atoms [7–9]. The He fluence for these studies was much lower (10^{16}–10^{17} He^+/m^2) and involved vacancy introduction by knock-on damage prior to He^+ irradiation to create well defined He trapping sites. In contrast, the present specimens were irradiated with much higher He^+ fluences (10^{21}–10^{24} He^+/m^2) without any prior creation of vacancy traps. However, since He^+ ions implanted below the damage threshold still form vacancy traps by ejecting 'self-interstitial atoms' (SIA) [8] and continue to grow by 'trap-mutating' with increased He filling [8], the initial trapping configuration loses meaning at high He^+ fluences (>10^{21} He^+/m^2) as He_nV_m complexes grow to form He platelets [11] and bubbles [13–15]. SEM images of W specimens irradiated with 8 keV He^+ at 873 K after thermal desorption show uniform hole structures [13] while the corresponding TDS spectra show one release peak at ~1000 K [13]. Therefore, the release peak at ~1000 K in the present study is attributed to He released from He_nV_m complexes or He bubbles. Post-irradiation imaging of the specimen surface was not performed in the present experiments, so the possible existence of He bubbles could not be confirmed. The third release peak at ~1200 K is discussed in Section 3.2.

Helium retention as a function of incident He^+ fluence obtained by integrating the area under the release rate vs. time curve is summarized in Fig. 3 for both 300 and 700 K irradiations. The relative uncertainty in the He retention values due to the profile integration procedure is estimated to be <10%. For 500 eV He^+ at 300 K, a fivefold increase in retention over three orders of magnitude increase in incident fluence is observed. The data labeled as (1) in Fig. 3 indicate a trend to saturation at a level of $\sim 5 \times 10^{20}$ He/m^2 for incident fluences above 10^{24} He^+/m^2. Similar retention levels are observed at much higher fluences (10^{25}–10^{26} He/m^2) at elevated temperatures [12] and will be further discussed in Section 3.2. Irradiations at 300 K with 2 keV He^+ resulted in a 2.5-fold increase in He retention compared to the 500 eV He^+ case at the same fluence; compare data (2) with (3) in Fig. 3. The enhanced retention observed for 2 keV He^+ may be due to additional vacancy trapping sites formed during irradiation by knock-on damage.

3.2. He^+-only irradiations at 700 K

For the 700 K irradiations the He^+ fluence range was narrower: $1.9–4.2 \times 10^{22}$ He^+/m^2. Similar to the 300 K cases, three desorption peaks were observed at ~500, ~1000 and ~1200 K; see Fig. 4. The peaks of profile (3) were shifted to higher temperatures due to an increasing nonlinear ramping rate during desorption – marked as 'nonlinear ramp' in Fig. 4. Despite the fact that the irradiation was done at 700 K, the first desorption peak at ~500 K is still

present. Initially, interstitial He that remained in the specimen and trapped upon cooling was suspected. Therefore, several specimens were held at 700 K for one hour following irradiation (labeled 'τ' in Fig. 4). Following this 'hold time', a reduction in the magnitude of the ~500 K peak was observed but not its entire removal. Tungsten irradiated with He plasmas at 873–933 K [12] and 700 or 1600 K [23] also exhibit this low temperature peak. This suggests that He^+ irradiation at elevated temperature involves some mechanism whereby He atoms in higher-energy traps are transferred to low-energy traps when the specimen cools.

The second He release peak is observed to vary between 980 and 1020 K (excluding profile (3) with nonlinear ramp). Irradiation with 2 keV He^+ causes an increase in the magnitude of this peak and an increase in the total amount of retained He; compare profiles (2) and (4) in Fig. 4 and data (5) and (7) in Fig. 3, respectively. This supports the earlier interpretation that He release at ~1000 K is from He_nV_m complexes or He bubbles, since increased vacancy creation from knock-on damage is expected for 2 keV He^+. Interestingly, the 'hold time' leads to ~65% reduction in retention for 500 eV He^+ while only ~10% reduction is observed for 2 keV He^+; compare data (4) with (5) and data (6) with (7) in Fig. 3, respectively. This result along with the similarity in the He desorption profiles (compare profiles (2) and (4) in Fig. 4), indicates that although energetically the He traps vary little between the high and low energy irradiations, there is a difference in the stability of the traps. Furthermore, for 500 eV He^+ irradiation, the 700 K specimen with τ has similar retention levels as the 300 K specimens; compare data (1) and (2) with (5) in Fig. 3. The higher retention levels observed for 700 K irradiation without τ may be a result of enhanced diffusion of He into the bulk. Further proof can be seen from elastic recoil detection (ERD) results presented in Fig. 6, Section 4.1.

A third release peak between 1150 and 1250 K is observed in some of the 700 K irradiations (see profiles (1) and (3) in Fig. 4) similar to the one 300 K case noted in Section 3.1. This third peak can be characterized by its rather sharp release but the randomness of the third peak makes it difficult to interpret the influence of hydrogen and deuterium on it. We note that A. van Veen [8] has observed He vacancy dissociation from various different configurations in this regime, albeit at much lower implanted He^+ fluences. The sharp release may indicate sequential dissociation [8] of He_nV_m complexes or bursting bubbles. Tokunaga et al. [12] have observed new desorption peaks at 1000–1200 K, when fine surface morphology changes in the form of island structures occurred in the tungsten specimens. Therefore, the appearance of this third peak in the present study may be an indicator that the He_nV_m complexes formed during irradiation were in transition to larger traps like bubbles.

4. Results and discussion: sequential irradiations

4.1. Sequential He^+–H^+ and He^+–D^+ irradiations at 300 K

4.1.1. Effect of H^+ (D^+) post-irradiation on He retention

TDS spectra of SEQ He^+–H^+ and He^+–D^+ irradiations at 300 K are presented in Fig. 5. The peaks at >800 K, characteristic of He^+-only irradiations, are not present; see Fig. 5(a) and (b). This indicates that the incident H^+ and D^+ ions have de-trapped the helium from the more energetic traps; compare profiles (1) and (2) with (3) in Fig. 5(a). Instead, He was found to desorb at 500 and 680 K, where D would normally be released for D^+-only irradiations; see profile (10) in Fig. 5(c). The absence of peaks >800 K suggests the elimination of He_nV_m complexes. This is consistent with the observations of Wang et al. [21] regarding He bubble removal following D^+ post-irradiation.

Helium release at 500 K is the only part of the TDS profile largely unchanged by post H^+ or D^+ irradiation. In Section 3.1 He released at 500 K was attributed to He trapped at grain boundaries or interstitial loops surrounding He_nV_m complexes. With the He_nV_m complexes now removed by D^+ post-irradiation, the unchanged 500 K peak suggests grain boundary trapping over interstitial loops. At present, it is unclear whether the He release at 500 K is from natural traps inherent in the specimen such as grain boundaries or traps formed by He_nV_m complexes. The previously unobserved release peak at 680 K may involve He trapping with D(H), but its reduction with increasing D(H) fluence suggests that it is a remnant of the He_nV_m complex; compare profiles (1) and (2) in Fig. 5(a) and profiles (4) and (5) in Fig. 5(b).

The ERD depth profiles in Fig. 6 indicate that at 300 K, the He is trapped within ~25 nm of the surface and the He distribution is centered at ~12 nm. This is 3× deeper than the calculated mean range of

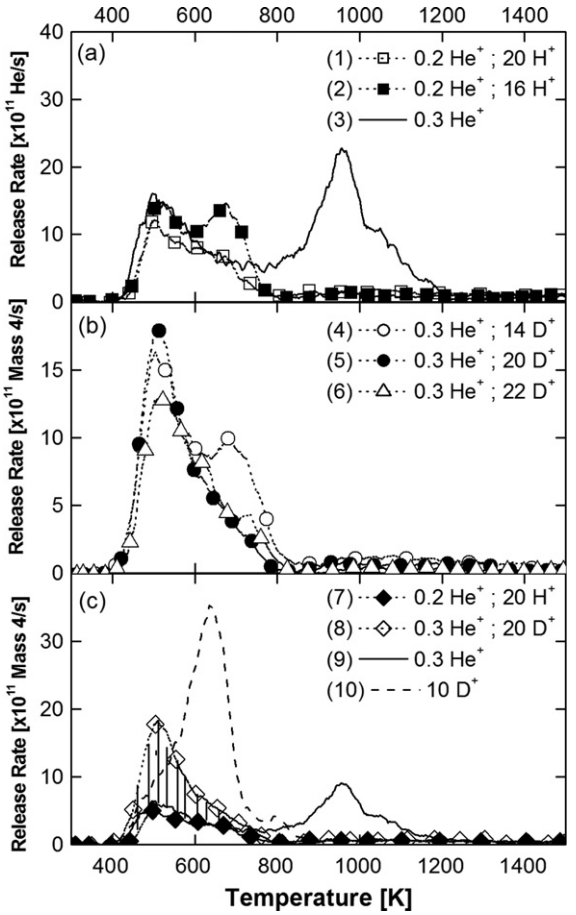

Fig. 5. TDS profiles for 500 eV SEQ irradiations at 300 K: (a) sequential He^+–H^+; (b) sequential He^+–D^+ and (c) comparison of two SEQ cases with D^+-only and He^+-only profiles. Temperature ramping rates were close to 3.0 K/s for all runs. The hatched area represents the D content due to SEQ He^+–D^+ irradiation, i.e., the difference between profiles (7) and (8). He release rates in (a) are based on He calibration and in (b) and (c) mass-4 rates are based on D_2 calibration. (Legend: fluences in units of $\times 10^{22}/m^2$).

4 nm using SRIM [30]. Since the He^+-only depth profile is unknown, it cannot be confirmed whether the increased He range is due to diffusion during He^+ irradiation or following D^+ post-irradiation. In any case, there is sufficient overlap with the D depth profile which also extends deeper than the SRIM calculated mean range of 7 nm.

4.1.2. Effect of He^+ pre-irradiation on D retention

The effect of the He^+ ions on D retention can be seen by taking the difference between the SEQ He^+–H^+ and He^+–D^+ profiles (profiles (7) and (8) in Fig. 5(c)). This difference shown by the hatched area

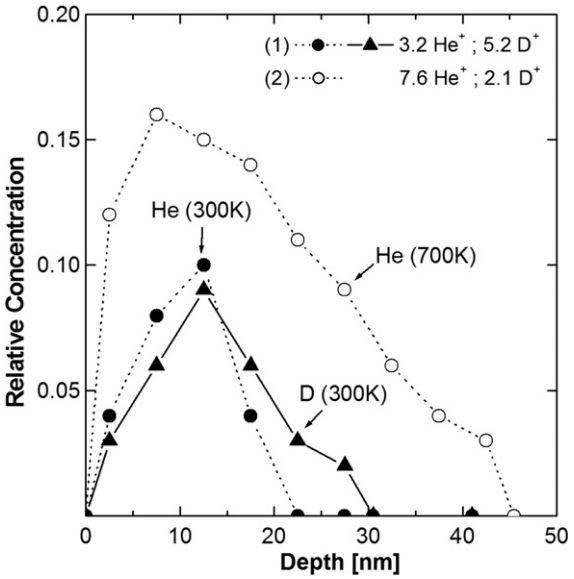

Fig. 6. ERD depth profiles for sequential 500 eV He^+–D^+ irradiations at 300 and 700 K. No D was observed for 700 K. ERD was performed by Dr. Dennis Whyte and Graham Wright at the University of Wisconsin, Madison. (Legend: fluences in units of $\times 10^{22}/m^2$).

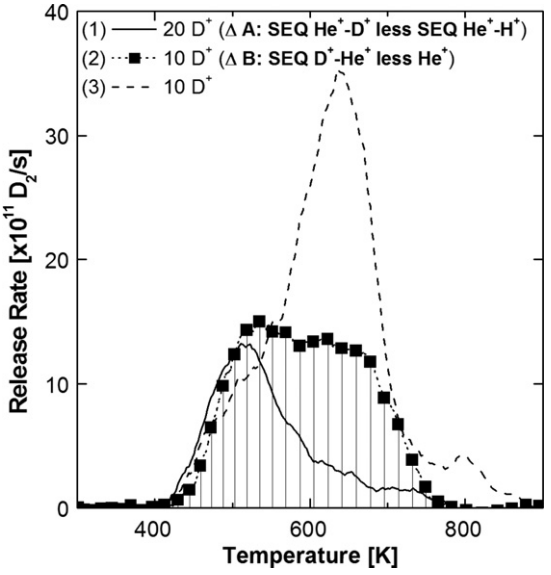

Fig. 7. All irradiations with 500 eV ions at 300 K. (1) TDS profile ΔA was obtained by subtracting SEQ He^+–H^+ (profile (7) in Fig. 5) from SEQ He^+–D^+ (profile (8) in Fig. 5); (2) TDS profile ΔB was obtained by subtracting He^+-only (profile (4) in Fig. 8) from SEQ D^+–He^+ (profile (1) in Fig. 8); and (3) TDS profile of a D^+-only implant obtained in the present study is shown for comparison. Temperature ramping rates during TDS were 2.5–3.2 K/s. (Legend: fluences in units of $\times 10^{22}/m^2$).

in Fig. 5(c) is also plotted in Fig. 7 (labeled as ΔA) along with ΔB (to be discussed below) and the D retention curve for D^+-only as reference. The ΔA curve clearly indicates that the post-irradiated D^+ is released at ~500 K, with the near-elimination of the 680 K peak. This D release at 500 K appears to be largely unaffected by the He presence and it is uncertain if there is any interaction between the trapped D and He. Yet, ion channeling experiments [31] of D implanted in He-damaged W indicate that D atoms are not trapped in their usual tetrahedral sites but randomly located with respect to the host lattice. This displacement indicates that He does have some effect on D trapping. Furthermore, others have also observed changes in this low temperature D release peak due to He presence [22,23]. So, it is possible that the deuterium breaks apart the He_nV_m complexes and re-traps interstitially with the He atoms.

The large reduction in D release observed in ΔA in the range 550–800 K (Fig. 7) translates to a ~70% reduction in total D retention compared to D^+-only irradiation. Comparison of deuterium depth profiles for the SEQ He^+–D^+ (ERD in Fig. 6) and the D^+-only implantations (SIMS in Fig. 1(b)) shows that D diffusion has been severely limited by the presence of He in the SEQ He^+–D^+ case. For SEQ He^+–D^+, D is trapped within a depth of ~35 nm, whereas for D^+-only, the D profile extends to >300 nm depth (Fig. 1(b) and [32]). From this we infer that the release of D in Fig. 7 between 400 and 800 K from SEQ He^+–D^+ irradiations must be from D trapped within ~35 nm of the surface. The overlap in depth for both He and D (Fig. 6) supports the idea that D is trapped with the He. Correspondingly, D release at 680 K observed for D^+-only must be in part due to D trapped deep in the bulk. Therefore, it is postulated that the reduction in D inventory for the SEQ He^+–D^+ irradiation is due to: (i) the limited diffusion of D into the bulk, and (ii) the possibility that D is unable to create vacancy traps in the near surface as the incident ion-energy is preferentially *consumed* to break apart the He_nV_m complexes. Most sequential irradiation studies have observed an increase in D retention with He^+ pre-irradiation [20,22]. The increase has been attributed to enhanced D trapping at defects surrounding He bubbles. With the elimination of He_nV_m complexes, as in the present case, it is not surprising that lower D retention is observed. Similar findings have also been reported by Nishijima et al. [23].

4.2. Sequential D^+–He^+ irradiations at 300 K

4.2.1. Effect of D^+ pre-irradiation on He retention

In Section 4.1 we presented results for sequential He^+–H^+(D^+) irradiation at 300 K and discussed the effects of post-irradiation by H^+ and D^+ on the desorption spectra and retained amounts of He and D. Here we present results where the sequence of irradiation was reversed; see Fig. 8 for SEQ D^+–He^+ at 300 K. Profiles for D^+-only and He^+-only irradiations are also plotted for comparison. The results indicate that in the temperature range 800–1200 K, where no D trapping/release is expected, the post-implanted He is unaffected by the presence of the pre-implanted D and is released in the same manner as in He^+-only irradiations; compare profiles (1) and (2) with (4) in Fig. 8. Therefore, it appears that the presence of D does not enhance the formation of He_nV_m complexes. Unfortunately, no SEQ H^+–He^+ irradiation was performed to confirm whether this was also the case for desorption in the 300–800 K range.

Helium release was also observed in the range 1700–2000 K, and for this one case, accounted for 10% of the total He retention; see profile (2) in Fig. 8. This is not exclusively due to D presence, since He^+-only irradiations have also shown release

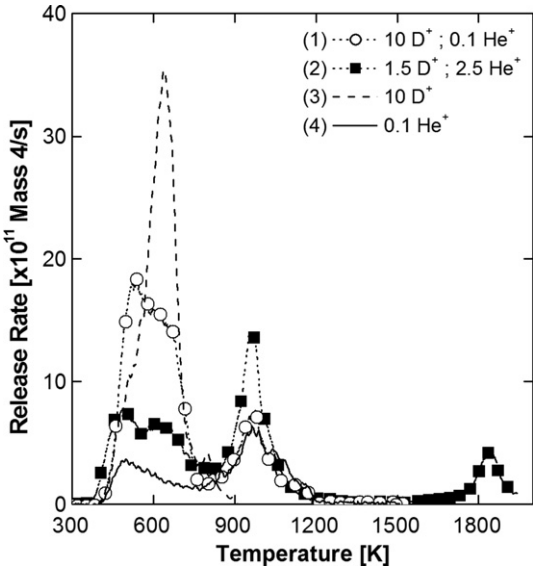

Fig. 8. TDS profiles for sequential 500 eV D^+–He^+ irradiations at 300 K. TDS profiles for D^+-only and He^+-only cases at the same energy and similar fluences are shown for comparison. Temperature ramping rates ranged from 2.8 to 3.6 K/s. Mass-4 release rates are based on D_2 calibration. (Legend: fluences in units of $\times 10^{22}/m^2$).

in the range 1600–2000 K when re-heated to 2000 K [27]. The He contribution from the re-heated experiments accounted for <1% of the total He retention. It is noted that the time interval between re-heating was four months. Therefore, the contribution to the He desorption profile and retention in the region >1500 K cannot be accurately determined from the present study. The helium release at >1500 K can also be from He bubbles or He_nV_m complexes with various He filling [4–9].

4.2.2. Effect of He^+ post-irradiation on D retention

Since no SEQ H^+–He^+ irradiations were performed, the He^+-only profile was subtracted from the SEQ D^+–He^+ profile in Fig. 8 to derive an approximate D retention behavior. The resulting ΔB profile, plotted in Fig. 7, represents the D content between 400 and 800 K. The observed reduction in the 680 K peak magnitude, compared to the D^+-only case, corresponds to ~40% reduction in D retention; compare profile (2) with (3) in Fig. 7. The 680 K desorption peak for the D^+-only implant was interpreted to be D trapped at vacancies at the near surface, and extended defects deep in the bulk [17,26,33]. Since ERD results have shown the He range to be limited to ~25 nm for 300 K implantations (see Fig. 6), the reduction in the 680 K peak is attributed to He de-trapping of D trapped at vacancies at the near surface. Hence, it can be inferred that during D^+-only irradiation with incident fluence of $\sim 10^{23}$ D^+/m^2, at least ~40% of the D retained is trapped at vacancies close to the surface.

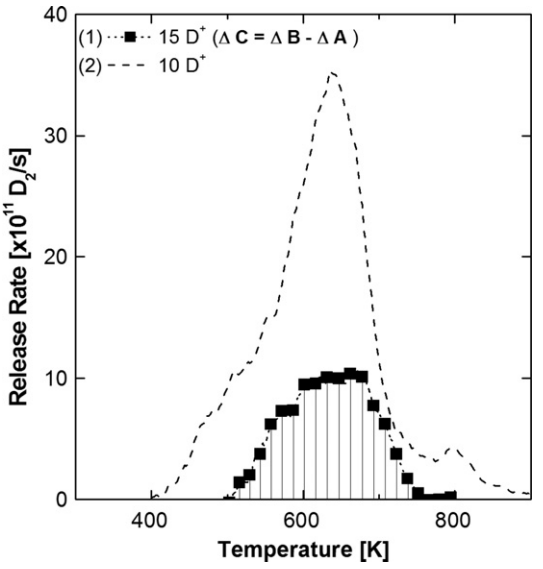

Fig. 9. TDS profile ΔC obtained by subtracting ΔA from ΔB in Fig. 7; ΔC is interpreted to be D trapped beyond ~35 nm. The profile for a D^+-only implant is shown for comparison. All profiles correspond to 500 eV irradiations at 300 K. (Legend: fluences in units of $\times 10^{22}/m^2$).

A portion of the remaining D release in the temperature range 400–800 K is interpreted to be D release from D trapped deep within the bulk beyond the He^+ implantation range. By taking the difference between the ΔB and ΔA profiles in Fig. 7 this amount can be separated; the resulting difference, ΔC, is plotted as profile (1) in Fig. 9. No depth profiles were obtained for the present SEQ D^+–He^+ cases, but judging from the D^+-only SIMS depth profile in Fig. 1(b), D is expected to be trapped well beyond the implantation range, extending to >300 nm. The D retention in the bulk, calculated by integrating the ΔC profile in Fig. 9 is $\sim 7 \times 10^{19}$ D/m^2, and when compared to the D^+-only case, accounts for ~30% of the total amount of D retained.

4.3. Summary of D trapping at 300 K derived from He^+pre/post-irradiations

The ΔA profile (Fig. 7) in the 400–600 K desorption range represents *D originating from D trapped within ~35 nm* of surface. The overlap of He and D ERD depth profiles suggests possible D–He trap configuration. Correspondingly, D release at 680 K (observed for D^+-only) is in part due to D trapping in the bulk. The D content in ΔA is $\sim 7 \times 10^{19}$ D/m^2, which represents ~70% less D retention than for D^+-only irradiation. This reduction is due to: (i) D unable to form vacancies at the near surface and (ii) D diffusion mitigated by the He presence.

The ΔB profile (Fig. 7) in the 400–800 K desorption range represents the *D loss from the near surface corresponding to the post-implanted He range of ~35 nm*. The D content in ΔB is $\sim 1.4 \times 10^{20}$ D/m^2, which represents ~40% less D retention than for D^+-only irradiation. The loss corresponds to a decrease in the 680 K desorption peak and thus to D trapped at vacancies at the near surface [17,26,33]. It is postulated that the post-implanted He^+ breaks apart the deuterium-vacancy traps.

From ΔA and ΔB, D trapped beyond ~35 nm can be estimated. The resulting ΔC profile (Fig. 9) in the 500–800 K desorption range represents *D originating from the bulk*. The D content in ΔC is $\sim 7 \times 10^{19}$ D/m^2, which represents ~30% of the total amount of D retained when D^+ is implanted alone.

4.4. Sequential He^+–D^+ irradiations at 700 K

The TDS spectra of sequential He^+-D^+ irradiation at 700 K are presented in Fig. 10. The entire QMS mass-4 release is attributed to He since no D was observed from ERD; see Fig. 6. For comparison, desorption profiles are also shown for SEQ He^+–H^+ irradiations at 300 K and He^+-only irradiations at 700 K. Profiles (3) and (4) clearly show that the post-implanted D^+ does not fully reduce the He desorption peak at ~1000 K. Furthermore, no He peaks are observed below 800 K. It is postulated that during D^+ post-irradiation, He is able to re-trap while D is unable to re-trap due to the high specimen temperature. This leads to the observed He release at ~1000 K but not at 680 K, which in Section 4.1, was attributed to He trapping with D. The He retention is 5.7×10^{19} He/m^2 and 7.1×10^{19} He/m^2 for profiles (3) and (4) in Fig. 10, respectively. Compared to the He^+-only irradiation, this is a 76% and 90% reduction, respectively.

The effect of τ is uncertain for the 700 K case. From Fig. 10, a 20% reduction in total He retention is observed for the case with τ (profile (3)) compared to the one without τ (profile (4)), but it is not possible to attribute this change entirely to a τ effect since the He^+ and D^+ fluences differed for the two cases.

4.5. Sequential D^+–He^+ irradiations at 700 K

TDS profiles for sequential D^+–He^+ irradiations at 700 K are presented in Fig. 11. The helium was implanted within seconds after the termination of D^+ irradiation. Yet, the pre-implanted D^+ is seen to have virtually no effect on the trapping behavior of He. Helium is observed to desorb in a similar manner as if it were implanted alone at 700 K; compare profiles (1) and (2) with (3) in Fig. 11. Furthermore, the total He retention for profiles (1) and (2) in Fig. 11 is 2.7×10^{20} He/m^2 ±2% and is 11% higher compared to He^+-only irradiations. Therefore, D^+ pre-implantation appears to have virtually no effect on subsequent He trapping. One possible effect of D is the consistent formation of the third peak compared to He^+-only irradiations at ~1200 K. As noted earlier in Section 3.2, the third peak may indicate the formation of larger He_nV_m complexes. It is expected that pre-implantation with D will result in some damage to the near surface – facilitating the growth of He_nV_m complexes. The temperature difference of ±50 K of the third peak is within experimental reproducibility but it is unclear if this is the reason for the observed shift, given the similar experimental conditions for profiles (1) and (2). Nevertheless, the TDS results are consistent with no D being trapped for 700 K irradiations.

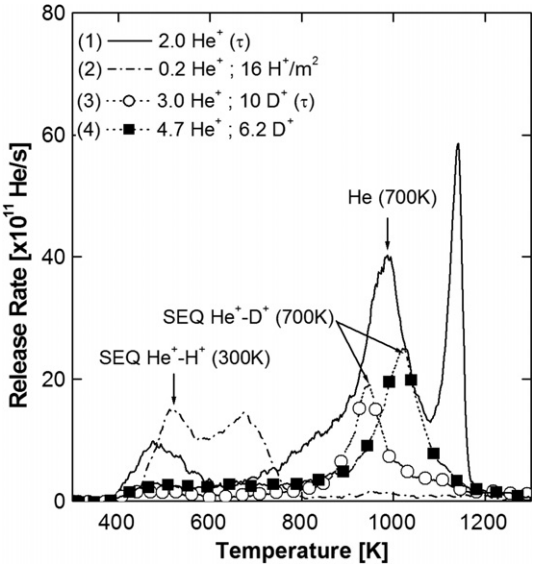

Fig. 10. TDS profiles for 500 eV SEQ He^+–D^+ irradiations at 700 K, with He^+-only at 700 K and SEQ He^+–H^+ at 300 K shown for comparison. Temperature ramping rates were 2.4–3.1 K/s. (Legend: fluences in units of $\times 10^{22}$/m^2).

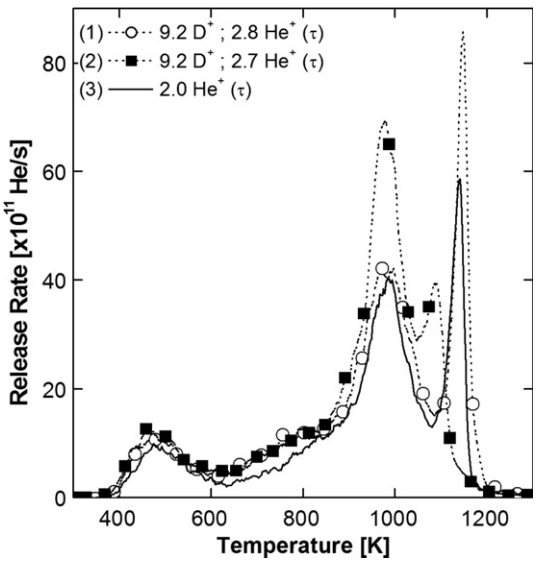

Fig. 11. TDS profiles for 500 eV SEQ D^+–He^+ irradiations at 700 K, with He^+-only at 700 K shown for comparison. Temperature ramping rates were 2.4–2.8 K/s. (Legend: fluences in units of $\times 10^{22}$/m^2).

5. Conclusions

5.1. He^+-only irradiations

Polycrystalline tungsten implanted with 500 eV He^+ ions at 300 K shows desorption peaks at ~500, ~1000 and ~1200 K. The helium is thought to form He_nV_m complexes or bubbles. He trapping at vacancies, by punching out self-interstitial atoms, appears to be the dominant trapping process. He retention increases slightly with increasing fluence, tending to saturation at $\sim 5 \times 10^{20}$ He/m^2 for incident fluences $>10^{24}$ He^+/m^2. Higher retention levels were observed for specimens implanted with 2 keV He^+. ERD profiles show trapped helium within ~25 nm and ~50 nm of the surface for 300 and 700 K irradiations, respectively; hence, He trapping at vacancy complexes can be reduced by post hydrogen irradiation.

For 700 K He^+-only irradiations the release peaks occurred approximately at the same temperatures as for 300 K. The release at ~500 K is still present despite the fact that irradiation was performed at 700 K, indicating some mechanism whereby He atoms in higher-energy traps are transferred to low-energy traps as the specimen cools. With the 1 h hold time (τ), He retention amounts for 700 K irradiations were similar to 300 K irradiations for 500 eV ions. However, without τ, He retention was ~2.5× higher; at least part of this increase is attributed to enhanced He diffusion. Overall, He^+ irradiation at 700 K does not significantly alter the 300 K trapping behavior of He in tungsten.

5.2. Sequential irradiations

Sequential He^+–D^+ irradiations at 300 K led to the elimination of He release peaks above 800 K. Instead, both D and He were released in the range 400–800 K. A single D peak at 500 K and two He Peaks at 500 and 680 K were observed; the 680 K He peak has not been seen previously from He^+-only irradiations in the present study. The D 500 K and He 680 K desorption peaks are interpreted to be due to a new trapping configuration involving interstitial deuterium and helium clusters in the near surface within a depth of ~35 nm. He pre-irradiation of the specimen resulted in a ~70% reduction in D retention in part due to the limited D diffusion into the bulk. Similar irradiation at 700 K resulted in a reduced single He peak in the range ~950–1050 K with very little release observed at <800 K. The post-implanted D is thought to de-trap and break apart the He_nV_m complexes, but the higher specimen temperature effectively disallows any He–D trapping.

Sequential D^+–He^+ irradiations at 300 K show that He trapping occurs in much the same manner as for He^+-only. Only D trapping in the near surface region is affected, with ~40% reduction in the total amount of D retained when compared to D^+-only. The loss is observed in the reduction of the 680 K peak in the TDS spectra, interpreted to be D release from vacancies in the near surface. The D in the bulk is largely unaffected and appears to contribute ~30% of the total D retained for 500 eV D^+ irradiations at 300 K. Similar irradiations at 700 K indicate that pre-irradiation with D^+ has little or no effect on the subsequent trapping behavior of He.

No modeling was performed in this study. However, D release from single-crystal tungsten under similar experimental procedures modeled by Poon et al. [34] using TMAP 7 [35] led to the identification of ~1.07, 1.34 and 2.1 eV traps corresponding to the 520, 640, and 900 K thermal desorption peaks, respectively.

Acknowledgements

This work was supported by the Natural Sciences and Engineering Research Council of Canada. We wish to thank Dr Dennis Whyte and Graham Wright at the University of Wisconsin, Madison, for the ERD measurements. We also thank Peter Brodersen at Surface Interface Ontario, University of Toronto, for performing the SIMS experiments and Charles Perez for his invaluable help with the experimental facility.

References

[1] G. Janeschitz, J. Nucl. Mater. 290–293 (2001) 1.
[2] G.J. Thomas, Radiat. Eff. 78 (1983) 37.
[3] S.K. Das, M. Kaminsky, in: M. Kaminsky (Ed.), Radiation Effects on Solid Surfaces, American Chemical Society, 1976, p. 112.
[4] K. Erents, G. Carter, Vacuum 16 (1966) 523.
[5] E.V. Kornelsen, Radiat. Eff. 13 (1972) 227.
[6] G.J. van der Kolk, K. Post, A. Van Veen, et al., Radiat. Eff. 84 (1985) 131.
[7] G. Carter, D.G. Armour, S.F. Donnelly, D.C. Ingram, R.P. Webb, in: S.F. Pugh (Ed.), Harwell Symp. on Inert Gases in Metals and Ionic Solids, AERE Report 9733, AERE, Oxfordshire, England, 1980, p. 83.

[8] A. van Veen, in: C. Abromeit, H. Wollenberger (Eds.), Vacancies and Interstitials in Metals and Alloys, Trans. Tech. Publ., Aedermannsdorf, 1986, p. 3.
[9] W.Th.M. Buters, J.H. Evans, A. van Veen, A. van den Beukel, Defects Diffus. Forum 57–58 (1988) 75.
[10] T. Hino, Y. Yamauchi, Y. Hirohata, J. Nucl. Mater. 266–269 (1999) 538.
[11] H. Iwakiri, K. Yasunaga, K. Morishita, N. Yoshida, J. Nucl. Mater. 283–287 (2000) 1134.
[12] K. Tokunaga, R.P. Doerner, R. Seraydarian, et al., J. Nucl. Mater. 313–316 (2003) 92.
[13] Zhang Fu, N. Yoshida, H. Iwakiri, Zengyu Xu, J. Nucl. Mater. 329–333 (2004) 692.
[14] D. Nishijima, M.Y. Ye, N. Ohno, S. Takamura, J. Nucl. Mater. 329–333 (2004) 1029.
[15] S.B. Gilliam, S.M. Gidcumb, N.R. Parikh, et al., J. Nucl. Mater. 347 (2005) 289.
[16] R. Sakamoto, T. Muroga, N. Yoshida, J. Nucl. Mater. 233–237 (1996) 776.
[17] M. Poon, A.A. Haasz, J.W. Davis, R.G. Macaulay–Newcombe, J. Nucl. Mater. 313–316 (2003) 199.
[18] A.A. Haasz, M. Poon, J.W. Davis, J. Nucl. Mater. 266–269 (1999) 520.
[19] V.Kh. Alimov, Phys. Scripta T108 (2004) 46.
[20] T. Hino, K. Koyama, Y. Yamauchi, Y. Hirohata, Fusion Eng. Design 39–40 (1998) 227.
[21] W. Wang, J. Roth, S. Lindig, C.H. Wu, J. Nucl. Mater. 299 (2001) 124.
[22] H. Iwakiri, K. Morishita, N. Yoshida, J. Nucl. Mater. 307–311 (2002) 135.
[23] D. Nishijima, T. Sugimoto, H. Iwakiri, et al., J. Nucl. Mater. 337–339 (2005) 927.
[24] A.A. Haasz, J.W. Davis, Nucl. Instrum. and Meth. B 83 (1993) 117.
[25] A.D. Quastel, R.G. Macaulay-Newcombe, J.W. Davis, A.A. Haasz, J. Nucl. Mater. 359 (2006) 8.
[26] M. Poon, Deuterium trapping in tungsten, PhD thesis, University of Toronto, 2004.
[27] H.T. Lee, Deuterium and helium trapping in tungsten under simultaneous irradiations, M.A.Sc. thesis, University of Toronto, 2005.
[28] H.T. Lee, A.A. Haasz, J.W. Davis, et al., J. Nucl. Mater., to be published.
[29] K. Erents, G. Carter, Vacuum 17 (1966) 97.
[30] J.F. Ziegler, J.P. Biersack, SRIM version 2000.40.
[31] S.T. Picraux, Nucl. Instrum. and Meth. 182–183 (1981) 413.
[32] A.A. Haasz, J.W. Davis, M. Poon, R.G. Macualay-Newcombe, J. Nucl. Mater. 258–263 (1998) 889.
[33] J.R. Fransens, M.S. Abd El Keriem, F. Pleiter, J. Phys. Condens. Mat. 3 (1991) 9871.
[34] M. Poon, A.A. Haasz, J.W. Davis, J. Nucl. Mater., submitted for publication.
[35] G.R. Longhurst, TMAP7: Tritium migration analysis program, User Manual, Idaho National Laboratory, INEEL/EXT-04-02352, 2004.